

 Open Access Full Text Article

ORIGINAL RESEARCH

Pulmonary toxicities from a 90-day chronic inhalation study with carbon black nanoparticles in rats related to the systemical immune effects

Chen Chu^{1,*}
 Lixiao Zhou^{1,*}
 Heran Xie^{1,*}
 Zijie Pei²
 Mengyue Zhang¹
 Mengqi Wu¹
 Shaohui Zhang³
 Luqi Wang⁴
 Chunfang Zhao⁵
 Lei Shi^{6,7}
 Ning Zhang¹
 Yujie Niu^{6,7}
 Yuxin Zheng⁸
 Rong Zhang^{1,7,*}

¹Department of Toxicology, Hebei Medical University, Shijiazhuang 050017, People's Republic of China; ²Department of Pathology, Medical School, China Three Gorges University, Yichang, 443002, People's Republic of China; ³Department of Experimental Center, The Third Hospital of Hebei Medical University, Shijiazhuang, 050051, People's Republic of China; ⁴Radiology, The Third Hospital of Hebei Medical University, Shijiazhuang 050051, People's Republic of China; ⁵Histology and Embryology, Hebei Medical University, Shijiazhuang 050017, People's Republic of China; ⁶Occupational Health and Environmental Health, Hebei Medical University, Shijiazhuang 050017, People's Republic of China; ⁷Hebei Key Laboratory of Environment and Human Health, Hebei Medical University, Shijiazhuang, People's Republic of China; ⁸Department of Toxicology, Public Health College, Qingdao University, Qingdao, 266000, People's Republic of China

*These authors contributed equally to this work

Correspondence: Rong Zhang
 Department of Toxicology, Hebei Medical University, 361 Zhongshan East Rd., Shijiazhuang, Hebei 050017, People's Republic of China
 Fax +863 118 626 5605
 Email rongzhang@hebmu.edu.cn

This article was published in the following Dove Press journal:
International Journal of Nanomedicine

Background: Recent years, there occurs heavy haze pollution in northern China during winter-time. The potential influence of airborne particulate matter (PM) on human health attracts great concern. The fuel-derived PM in the inhalable size range is dominated by aggregates of nanoparticles of Carbon black (CB). However, there are still lack of evidences especially regarding long-term exposure to explain the chronic effects of nanoscaled CB and the relative mechanism.

Purpose: The objective of this study was to identify the potential mechanism of chronic effects of nanoscale CB. The systemic toxicity, immune suppression or activity and local toxicity were evaluated.

Methods: 32 rats were divided into 2 groups: 30 mg/m³ CB exposure (nose only, 90 d, 6h/d) and control (clean air). Half of rats were scarified after exposure and another half of rats recovered for 14 days. Eight rats in each group were executed the lung function tests using a ventilated bias flow whole body plethysmograph (WBP). SDS-PAGE protocol was used to detect the deposition and retention of CB in lung of rats. HE staining was used to observe the changes of histopathology. Cell apoptosis was examined by TUNEL assay or flow cytometry. The levels of IL-6, IL-8, IL-17 and TNF- α in serum and lung tissue were evaluated with commercially available ELISA kit. The peripheral blood cell counts were detected by Auto 5-diff hematology analyzer.

Results: The lung burden of CB was 16 mg in lung of rats after a 90-day exposure by MPPD. Fourteen percentages of the amount of CB accumulated at the end of the exposure period was cleared from the lung during the 14 dys recovery period. The lung function was significantly decreased and could not recover after a short time recovery. The fibroblasts and granuloma formation were found in lung. The levels of apoptosis and DNA damages were significantly increased in lung cells after CB inhalation. The cytokines levels in lung but not in serum were significantly increased in CB exposure group. The cell counts of WBC, monocytes and neutrophils had 1.72, 3.13, and 2.73-fold increases after CB exposure, respectively. The percentages of CD4+ lymphocytes and the rates of CD4+/CD8+ were statistically increased after CB exposure. The stimulation indexes of the peripheral blood lymphocytes were significantly decreased after CB exposure. In the CB exposure group, the disrupted histomorphology of thymus and spleen were found as well as the early apoptotic thymocytes had a 2.36-fold increase.

Conclusion: CB induced the localized or direct toxicity and systemic immune toxicity. The direct and systemic immune responses had a combined effect on the lung damages caused by CB.

Keywords: nanoscale CB particles, pulmonary toxicology, immune toxicity, chronic toxicity, inhalation

Introduction

Recently, the potential influence of airborne particulate matter (PM) on the environment and human health attracts great concern.¹ Combustion-derived carbonaceous aerosols have traditionally been associated with pollution in urban areas.² Emissions of carbonaceous matter in China have increased by approximately 20% from 1996 to 2010.³ In the north of China, 46% contribution of the monthly average PM2.5 concentration was residential coal burning.⁴ The recent studies suggested that the formation of haze in northern China during wintertime was attributed to the primary emissions from residential coal burning.^{5,6} Because it is difficult to determine the weighting coefficient of each component to the overall toxicity under different settings because of the complicated composition of airborne particles,⁷ the study on the characteristics of primary particles from residential coal burning has been necessary. Black carbon (originates from incomplete combustion of fossil and biomass fuels and represents an important constituent of atmospheric aerosols, with an estimated global emission rate of 4.3–22 Tg·year⁻¹).⁸ In occupational environment, the concentration of carbon could reach 15 mg/m³.⁹

The fuel-derived PM in the inhalable size range is dominated by aggregates of nanoparticles of Carbon black (CB).¹⁰ Nanoscale CB (Printex 90) at the concentration of 11.7 mg/m³ caused lung tumors in rats after 2 years of inhalation.¹¹ However no information of detailed deposition, clearance, and retention was provided. In spite of plenty of evidence of adverse effects induced by CB particles, according to the report of overall reevaluation to CB by IARC in 2010, the mechanistic information of the diseases induced by CB is still does not clear enough based on current evidence.¹²

Two main kinds of toxicities may exist due to CB exposure: Localized and systemic toxicities.¹³ In fact, systemic toxicity involves an immune response that causes damage to the lungs.^{14–16} The immunotoxic potential and ability of nanoparticles to alter immune responses has been documented.^{17–19} Frampton et al, reported that CB exposure increased neutrophils and decreased monocytes and basophils among healthy adults after exposure to 25 µg/m³ of ultrafine carbon particles for 2 hrs.²⁰ Intratracheal instillation of 14 and 95 nm CB in mice caused pulmonary inflammation. It triggered the induction of proinflammatory cytokine and chemokine release in the lung as well as translocated to the mediastinal lymph nodes.²¹ Previous research has shown that exposure to 0.2 mg/mouse CB nanoparticles by intranasal route can contribute to immunological responses, including allergy.²² Airway exposure to

CB nanoparticles induces pulmonary inflammation, affects allergy associated T helper (Th2) cytokine bias²³ and induces genotoxic damage.²⁴ In animal models, acute respiratory, subcutaneous and direct immune cell exposure to CB nanoparticles enhances allergy to chicken egg ovalbumin protein.^{25,26} However, because of the short-term exposure, it is uncertain whether the observed chronic changes in blood cell counts constitute adverse health effects or reflect a normal immune response to these environmental stimuli in healthy individuals. In our previous study, the elevated levels of pro-inflammatory cytokines in CB packing workers after 15 mg/m³ CB exposure were found. We observed statistically significant increases of cytokines interleukin-6 (IL-6), interleukin-8 (IL-8), interleukin-17 (IL-17), tumor necrosis factor alpha (TNF-α), and Macrophage inflammatory protein-1.⁹ Eosinophils were reported to be increased in workers exposed to nanoscaled CB particles for an average of 11.5 years but we did not observe the statistically significant differences in lymphocytes and monocytes.²⁷

Therefore, there is still a lack of evidence especially regarding long-term exposure to explain the chronic effects of nanoscaled CB and the relative mechanism. The localized and systemic toxicities involved immune response after short-time CB exposure contributed to the damages of lung.^{13–16} Though there were significantly different responses and mechanisms between short term and chronic toxicity of particles, the inflammation, and immune responses were found in long-term CB exposure workers.^{9,27} Therefore, our hypothesis is chronic inflammation triggered by immune response could contribute to the toxicity of CB. In the present study, we established a 90-day nose-only inhalation CB model in rats to explore the possible mechanisms. The systemic toxicity, immune suppression or activity, and local toxicity were evaluated. Our results suggested that the direct and systemic immune responses had a combined effect on the lung damages caused by CB. Data collected from the present study will serve to explore health effects related to PM components and might provide strategies that reduce diseases induced by particle materials.

Material and methods

Animals and CB exposure study design

Male, pathogen-free Sprague–Dawley rats at 6 weeks of age were acclimated for a week before the commencement of inhalation exposure. During the acclimation and inhalation

exposure, the rats were housed in polycarbonate cages and provided food and tap water ad libitum in a controlled humidity and temperature environment with a 12 hrs light/dark cycle. We divided 32 rats into two groups: control and exposure. Rats in the exposure group were exposed to CB in the nose-only inhalation chamber at 30 mg/m^3 for 6 hrs/day for 90 days. The control animals were exposed to filter air for 24 hrs/day. After exposure for 90 days, eight rats were selected randomly and scarified in each group, respectively. The rest eight rats in each group were recovered for 14 days after exposure in the chamber with HEPA-filters. Rats were anesthetized by pentobarbital sodium and sacrificed at the endpoint of treatment. Blood samples were collected from abdominal aorta. Organs were separated to further detect. The present protocol was approved by the Committee of the Ethics Animal Experiments of Hebei Medical University (IACUC-Hebmu-20160047) and carried out under the Hebei Medical University institutional guidelines for ethical animal use.

Characterization of CB, aerosol generation, and conditions in the inhalation chamber

CB ($\geq 99.8\%$) was purchased from the CB manufacturing factory (Jiaozuo Chemical Industry Limited Company, Henan, China) and its characteristics were the same as our previous studies.^{9,27} Briefly, Tecnai G220 transmission electron microscope (TEM, FEI, USA) and Sirion

200 scanning electron microscope (SEM, FEI, Holland) were used to evaluate the size and morphology of CB particles. Nitrogen adsorption capacity was calculated to evaluate the specific surface characteristics of CB by Brunauer–Emmett–Teller method. The size and zeta potential of CB particles were performed on DelsaTM Nanoparticle analysis instrument (Beckman coulter, CA, USA).

CB was baked at 80°C for 12 hrs before exposure and packed in an aerosol generator column (Beijing Huironghe Technology Co., Ltd. Beijing, China). The aerosol generator system was employed to reliably disperse non-cohesive powders such as mineral dusts, medical compounds, pollen, and so forth in the size range $<100\text{ }\mu\text{m}$. In the present study, the CB powder was filled into the powder reservoir and uniformly compressed along a 20 cm filling height by a tamper. Then, the CB powder was transported onto a rotating brush at 13 L/min feed rate. The powder that came from the reservoir and had been loosened from the rotating brush was dispersed into practically all individual particles at 23 L/min speed in the dispersion head by dispersion air at 10 L/min flow rate. Dosing was performed using a precisely controlled feed rate of the feed piston (Figure 1). The concentration of CB aerosol in the exposed chamber was $22.50\text{--}42.50\text{ mg/m}^3$ by filter weighing method, and the average was $30.06 \pm 4.42\text{ mg/m}^3$ (Supplemental Figure S1A and S1B). During exposure, each rat was placed in

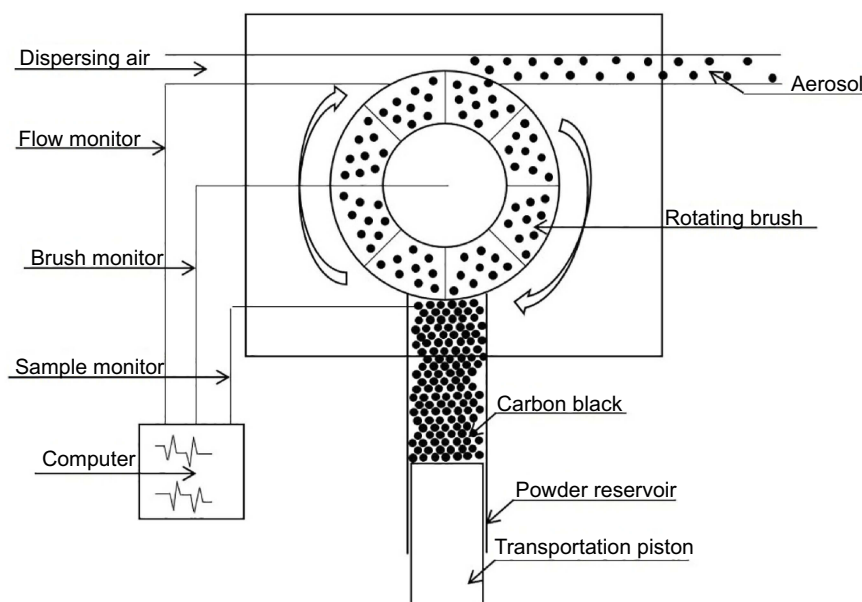


Figure 1 The diagram of the aerosol generator structure.

a polycarbonate holder and constrained with a sealed restraint inserted in the rear opening of the holder so that only the tip of the rat's nose projects out of an opening in the front of the holder.

A prediction of the deposited alveolar fraction was generated using the MPPD model version 3.04.²⁸ The calculated deposition fraction of SD rats was 0.1146, and the deposition in each rat was 16 mg by MPPD after CB exposure for 90 days. At the occupational exposure limit of 3.5 mg/m³ CB per 8 hrs work shift (established by the Occupational Safety and Health Administration and the National Institute for Occupational Safety and Health), the deposition in each worker was 80 mg by MPPD after CB exposure for 90 days.

Lung function test

Eight rats in each group were executed the lung function tests using a ventilated bias flow whole body plethysmograph (AniRes2005, Beilanbo Ltd, China). The parameters of lung function included the percent predicted forced expiratory volume in 1 s (FEV1), forced vital capacity (FVC), FEV1/FVC (%), percent predicted peak expiratory flow (PEF), and percent predicted maximal midexpiratory flow curve (MMF). The rats were placed in the animal chamber, and the plethysmography was then conducted based on the measurements of the selected parameter values for 5 mins.

Detection of pulmonary deposition/clearance by SDS-PAGE

According to the previous literature with a small modified SDS-PAGE protocol was used to detect the deposition and retention of CB in rats.²⁹ Six lungs of rats in each group were used to detect the CB contents. Thirty milligram lung tissue was homogenized in 700 µL normal saline and then processed for SDS-PAGE. The optical images of gels were acquired using a flatbed scanner (Tanon-5500, Tanon Science& Technology Co., Ltd. Shanghai, China) and the optical density (OD) of each band, which represented the CB contents, was quantified using Image-Pro Plus 6.0 software (Media Cybernetics, Inc. Rockville, MD). (Supplemental methods).

Organ coefficient and histopathological examination

Organs, including testis, heart, lungs, kidneys, spleen, liver, and brain were separated and weighted at the endpoint of the experiment. The organ coefficient of eight

rats in each group was calculated according to the formula: organ weight/body weight ×100%. Six rats in each group were used to histopathological examination. The animal's noses were perfused via the nasopharyngeal opening with approximately 5 mL of formalin, trimmed of excess soft tissue, and immersion-fixed in 10% neutral buffered formalin. After decalcification, the noses were cut transversely perpendicular to the bridge of the nose. The lungs, spleen, and thymus were immersion-fixed in 10% neutral buffered formalin for 24 hrs and then embedded in paraffin. Following paraffin embedding, tissues were cut into 5 µm serial sections. Hematoxylin and Eosin staining was used to observe the changes in histopathology.

Lung sections were stained with Masson following the manufacturer's protocol (Sigma–Aldrich, Missouri, USA). Briefly, the samples were stained with iron hematoxylin, Ponceau-acid fuchsin solution and phosphomolybdic acid solution sequentially, and then stained with aniline blue. Images were observed under a light microscope (Olympus, Japan).

The scoring criteria were as follows: a) alveolar congestion, b) fibrin exudation, c) desquamation of alveolar epithelial cells, d) infiltration or aggregation of neutrophils in airspace or vessel wall, and e) thickness of alveolar wall. Six rats in each group and each item was scored on a 5-point scale as follows: 0=minimal damage, 1=mild damage, 2=moderate damage, 3=severe damage, and 4=maximal damage.

For TEM image, three animals in each group were deeply anesthetized and perfused with 20 mL of 37°C saline solution. After perfusion with 100 mL of 4°C 2.5% glutaraldehyde in 4% paraformaldehyde, the lung was cut into 1 mm³ pieces, fixed and embedded in 100 EPON for 48 hrs at 70°C. Ultra-thin sections of 70 nm were cut and stained with or without 2% uranyl acetate and lead citrate, and examined under H-7500 TEM (Hitachi, Japan).

The apoptosis detection

Following paraffin embedding, six lungs of rats in each group was cut into 5 µm serial sections, and apoptosis was examined by TUNEL assay according to the manufacturer's protocol (Roche Ltd., Shanghai, China). Briefly, Apoptotic indices (OD) were calculated as TUNEL-positive cells by Image-Pro plus 6.0 software (Media Cybernetics, Inc. Rockville, MD).

The apoptosis of thymocytes was detected using flow cytometry. About 1×10⁶ thymocytes per milliliter were harvested and resuspended in 100 µL binding buffer.

Annexin V coupled with FITC was added according to the AnnexinV-FITC kit (Becton Dickinson, USA). Following 30 mins of incubation at room temperature in darkness, 50 µg/mL Propidium Iodide was added and incubated for 1 min before FACS analysis (lymC6 flow cytometer, Becton Dickinson, USA). Data from 1×10^4 cells were collected and analyzed in each sample.

Cytokines analysis by enzyme-linked immunosorbent assay (ELISA) and immunohistochemical staining (IHC)

For ELISA, 0.5 g lung tissues from six rats in each group was homogenized in 700 µL saline solution and then centrifuged at $700 \times g$, respectively. The supernatants were collected and analyzed. The levels of IL-6, IL-8, IL-17, and TNF- α in serum and lung tissue were evaluated with commercially available rat ELISA kit according to manufacturers' recommendations (NeoBioscience, Shenzhen, China).

For IHC, antigenic site retrievals were accomplished by a microwave heat-mediated method and incubation with 10 mmol/L citrate buffer (pH 6) for 12 mins. Sections were incubated in 3% hydrogen peroxide for 10 mins; washed three times (3 mins each) with 0.01 mmol/L PBS (pH 7.4); and blocked with goat serum. The slides were subsequently incubated overnight at 4°C with the following antibodies: IL-8, IL-6, and IL-17 (1:100; Bioworld, Nanjing, China). The sections were washed with PBS (three times for 3 mins each). Slides were then treated with an anti-rabbit secondary antibody (ZSGB-Biology, Beijing, China) and developed using avidin-conjugated HRP with diaminobenzidine as a substrate (ZSGB-Biology), followed by hematoxylin counterstaining. Images were observed under a light microscope (Olympus Ltd., Japan). The OD value was quantified using Image-Pro Plus 6.0 software. For IL-8, IL-6, and IL-17 staining analysis, the integrated optical densities (IODs) of the positively stained areas of six consecutive high-power fields in one section at $400 \times$ magnification was determined, and the IODs from a total of five sections (six rats) in each group were averaged.

The analysis of peripheral blood cell counts and lymphocyte subsets

The peripheral blood cell counts were detected by Auto 5-diff hematology analyzer (Tecom Science Corporation, Nanchang, China). Peripheral lymphocytes from six rats in each group

were isolated using lymphocyte separation solution (Solarbio Life Sciences Co., Beijing), respectively. Briefly, 100-µL lymphocytes with a concentration of 1×10^6 cells/mL were incubated with the antibody combination of CD3 with CD4, CD3 with CD161, or CD3 with CD8 (BD Biosciences, San Jose, CA), respectively. The final concentrations of CD4, CD3, and CD8 were 1, 2, and 1 µg/mL, respectively. The samples were incubated for 20 mins at room temperature in the dark. After PBS washed twice, the fluorescent intensity of 10,000 lymphocytes per sample was acquired using AccuriC6 flow cytometer (Becton Dickinson, USA).

The lymphocytes proliferation was detected as follows: 100 µL of the lymphocytes suspension at a final concentration of 5×10^5 cells/mL was incubated in quadruplicate in 96-well plates. A working concentration of 50 µg/mL phytohaemagglutinin (PHA) was used for the stimulation of lymphocytes and for corresponding control. After 48 hrs of incubation at 37°C in the 5% CO₂ incubator, 20 µL of MTS (Madison, WI USA) were added to each well. The cells were incubated for another 4 hrs, and then 150 µL of DMSO was added to each well. The OD value was read on a multiwall scanning spectrophotometer (SynergyTM HT, BioTek Instruments, Inc., USA) at 570 nm. Stimulation index (SI) was calculated as SI = At/Ac, where At is the absorbance of the sample stimulated by PHA and Ac is the absorbance of sample without stimulation by PHA.

Statistical analysis

Data management and statistical analysis were performed using Statistical Package for Social Sciences (SPSS) vs 21.0 (SPSS Inc., Chicago, IL, USA). Two-group *t*-test was used to compare the difference between CB exposure, recovery, and their respective control, respectively. The comparison between the CB exposure, recovery, and the controls was analyzed using one-way analysis of variance followed by the Dunnett's multiple comparison test when *F* was significant compared to the recovery group. Non-parametric statistics were performed to compare the pathological score (Mann-Whitney *U*-test). The Differences were considered significant when *P*<0.05.

Results

The physicochemical parameters of the CB and its deposition

SEM examinations indicated that particles ranged from 30 to 50 nm and the agglomeration of particles ranged from 200 to

400 nm in size. TEM confirmed that the CB particles contained clusters comprised of smaller particles, 30–50 nm in size. In water, the hydrodynamic size of particles ranged from 200 to 400 nm. The nitrogen adsorption capacity was 74.85 m²/g, and the Zeta potential was −15.37 (MV).

The contents of CB in lung tissue were 7.09 mg after 90-day exposure and 6.09 mg after 14-day recovery (Figure 2). Fourteen percentages of the amount of

CB accumulated at the end of the exposure period was cleared from the lung during the 14-day recovery period.

The pulmonary toxicity caused by chronic CB exposure

At CB exposure 21 days, statistically significant differences of body weight were found between CB exposure

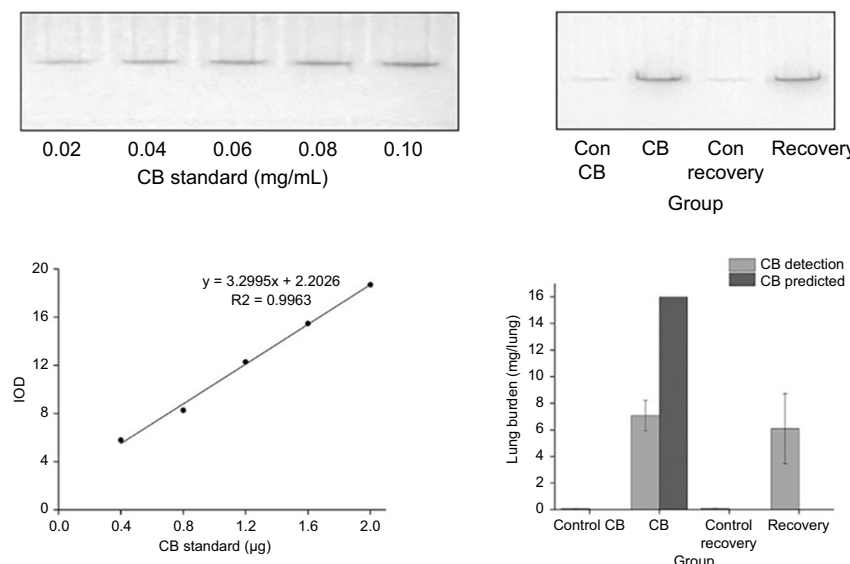


Figure 2 Quantitation of Carbon black (CB) extracted from lung tissue by SDS-PAGE and optical images. On the top of graphs, a representative gel was loaded with known CB standards in lanes 1–5 and lung lysates in lanes 6–8. On the bottom of left graph, there was the plot of CB standard content determined from corrected mean pixel intensities of the CB-containing bands as a function of CB concentration. On the right of bottom graph, there was the lung burden of CB in each lung of rat according to the equation $Y=3.2995X+2.2026$. Data were shown as the mean \pm SD (standard deviation). n=8.

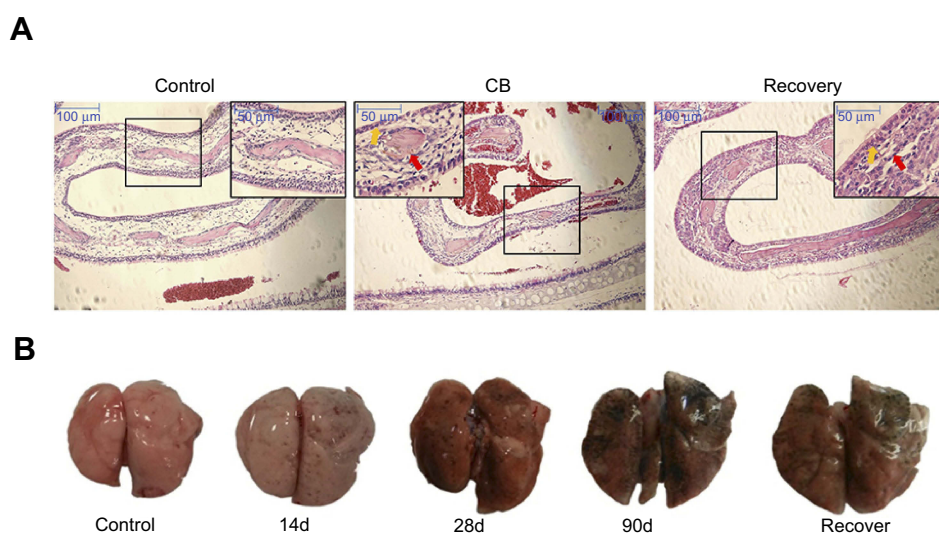


Figure 3 Images of the turbinate bone and the lung in rats. **(A)** Representative photomicrograph of pathological changes in the turbinate bone in rats. (HE staining, 100×, 200×). The red arrows indicate atrophy or thinning of the olfactory epithelium. The yellow arrows indicate inflammation cells. **(B)** Images of lungs.

Abbreviation: CB, Carbon black.

and the control group ($t=5.387, P=0.000$) (Supplemental Figure S2). After CB nose-only exposure for 90 days, the olfactory epithelium was atrophied and thinning which cannot recover in a short time (Figure 3A). At the terminal necropsy, the pigment was found in lung surface. After recovered for 14 days, the lung still looked dark (Figure 3B). The lung coefficient in the CB exposure group and recovery group was significantly increased compared to the control ($t=3.357, P=0.004; t=2.334, P=0.038$, respectively) (Supplemental Table S1). More CB particles were deposited in the lung interstitial than the alveolar cavity in CB exposure group. There were no CB-specific macroscopic findings in the other organs.

The macrophages with phagocytized CB particles were accumulated in the pulmonary interstitium (Figure 4) and pulmonary lymph node (supplemental Figure S3). The thickened alveolar wall, widened lung space, telangiectasia congestion, and abnormal endotracheal mucosal epithelial cells were found in lung tissue of rats after CB inhalation. There was granuloma formation near bronchioles and adjacent alveoli consisting of round clusters of large macrophages and multinucleated giant cells that contained abundant amorphous pigment. Many of these granulomas contained numerous polymorphonuclear cells (pyogranulomas), and some extended from the alveoli into the wall and lumen of the bronchiole. The

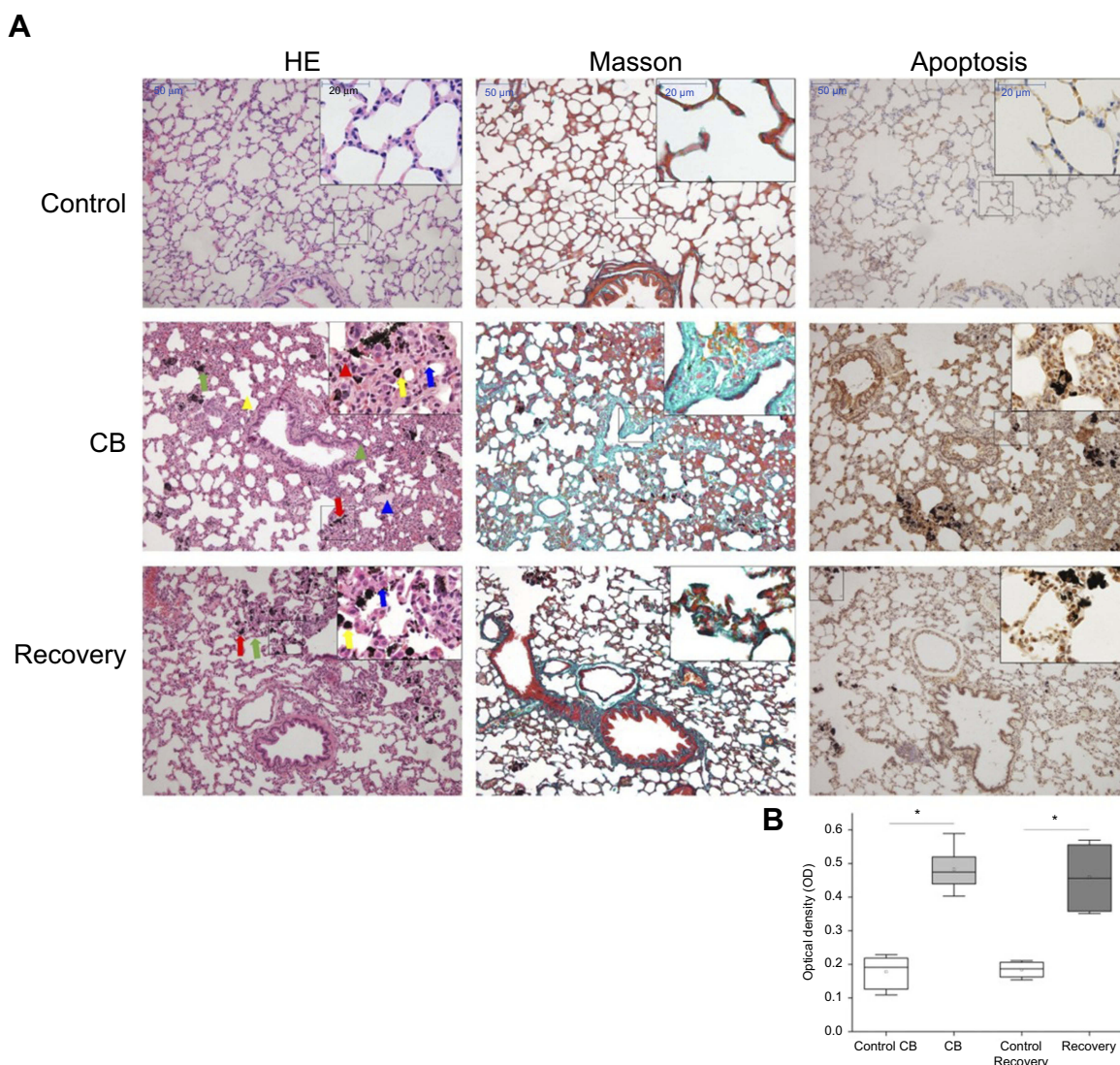


Figure 4 Representative histopathological images and the apoptosis of lung tissue in rats. **(A)** Representative histopathological images stained by HE and Masson as well as apoptosis by TUNEL. Inset: a higher magnification of the lung tissue (400×). The arrows indicate: Red arrow, CB particles in pulmonary alveoli or bronchiole; Yellow arrow, macrophages with CB particles; Blue arrow, granuloma; Green arrow, alveolar walls and pulmonary mesenchyme thickened; Red triangle, inflammatory cells; Yellow triangle, alveolar fusion. Blue triangle, serous inflammation; Green triangle, abnormal endotracheal mucosal epithelial cells. **(B)** Apoptosis levels in the lung of rats induced by CB. * $P<0.05$ compared with the control group. # $P<0.05$ compared with the CB exposure group. Data were shown as the mean ± SD. n=6.

granulomas circumscribed areas of fibrosis that extended for a short distance into surrounding septal walls. The inflammation, including macrophages, mononuclear cells, and lymphocyte infiltration, was found in pulmonary interstitium in CB exposure group.

Focal fibrosis (Figure 4), characterized by thickening and size increase of collagen fibers was often associated with the granulomatous changes after CB inhalation. The degree of phagocytosed CB particles accumulation, inflammation, focal fibrosis, and other histopathologic changes in the lung of the rats in the recovery group was almost similar to the CB exposure group. The score in CB exposure recovery group showed a statistically significant elevation than that of the control ($U=10.000, P=0.000$) (Table 1).

The image of the apoptotic cells is shown in Figure 4. Compared with the control, the apoptosis in lung tissue of rats had 2.72, 2.51-fold increases in CB exposed and recovery group, respectively. Compared with the CB exposure group, there was no significant decrease in the recovery group. (Figure 4B). Compared with the control, the DNA damage in lung tissue of rats had 10.38, 9.15-fold increases in CB exposed and recovery group, respectively (Supplemental Figure S4).

The image of TEM showed particles in the alveolar space and macrophages (Figure 5). For removing the background of uranyl acetate and lead citrate staining, we observed a large number of particles in macrophages. In alveolar type II epithelial cells, the microvillus and the osmophilic multilamellar body disappeared, perinuclear spaces widened, and organelles reduced. The fibrosis was found in the blood-gas barrier (supplemental Figure S5).

The cytokines of inflammation in the lung were detected by ELISA and IHC. Our data showed the IL-6, IL-8, IL-17, and TNF- α levels in lung were statistically increased in CB

exposure group compared with the control ($t=6.584, P=0.000; t=5.364, P=0.000; t=3.859, P=0.001; t=3.227, P=0.002$; respectively) (Table 2, Supplemental Figure S6A and S6B). After a 14-day recovery was given, IL-8 and TNF- α in the lung homogenate only had slight decrease compared with the CB treatment group and still statistically higher than that of the control group ($F=18.696, P=0.008; F=35.415, P=0.000; F=23.237, P=0.003; F=41.336, P=0.000$, respectively). The IL-6 and IL-17 levels were no significant increases in recovery group compared to the control, but the decreases were significant when compared with the CB exposure group.

The results of lung function tests are shown in Table 3. Exposure to CB was associated with a significant reduction in FEV1, FEV1/FVC, MMF, and PEF when compared with the control group ($t=3.487, P=0.006; t=3.964, P=0.003; t=4.096, P=0.004; t=2.145, P=0.018$; respectively). The means of FEV1, FVC, FEV1/FVC (%), PEF, and MMF had 26.95, 19.01, 9.78, 17.52, and 19.61% decrease in the CB exposure group compared with the control, respectively. The recovery rats also had significant decrease in FEV1, FVC, FEV1/FVC (%), PEF and MMF compared with the control group ($t=3.262, P=0.007; t=4.904, P=0.001; t=3.254, P=0.008; t=2.856, P=0.013; t=2.552, P=0.022$, respectively). The means of FEV1, FVC, FEV1/FVC (%), PEF, and MMF had 23.34, 13.18, 11.70, 10.68, and 13.14% decrease in the recovery group compared with the control, respectively.

The systemic inflammation and immune responses induced by CB

The results of hematology analysis and lymphocyte subsets are shown in Table 4. After CB inhalation for 90 days, the peripheral blood cell counts of White Blood Cell

Table 1 Summary of significant histopathological findings in the lung of rats after CB exposure

Histopathological findings	Control CB	CB	Control Rec	Recovery
Alveolar congestion	0.27±0.23	2.47±0.12	0.24±0.22	2.60±0.20
Fibrin exudation	0.13±0.12	3.4±0.20	0.08±0.07	2.93±0.12
Desquamation of alveolar epithelial cells	0.47±0.31	2.67±0.23	0.54±0.40	2.47±0.23
Infiltration or aggregation of neutrophils in airspace or vessel wall	0.07±0.20	2.20±0.40	0.08±0.12	2.20±0.20
Thickness of alveolar wall	0.07±0.12	3.53±0.23	0.13±0.10	3.00±0.20
Total score	1.00±0.23	14.27±0.23*	1.07±0.18	13.20±0.60**#

Notes: The number of rats in each group was six and data were shown as the mean ± SD. * $P<0.05$ compared with the control group. ** $P<0.05$ compared with the CB exposure group.

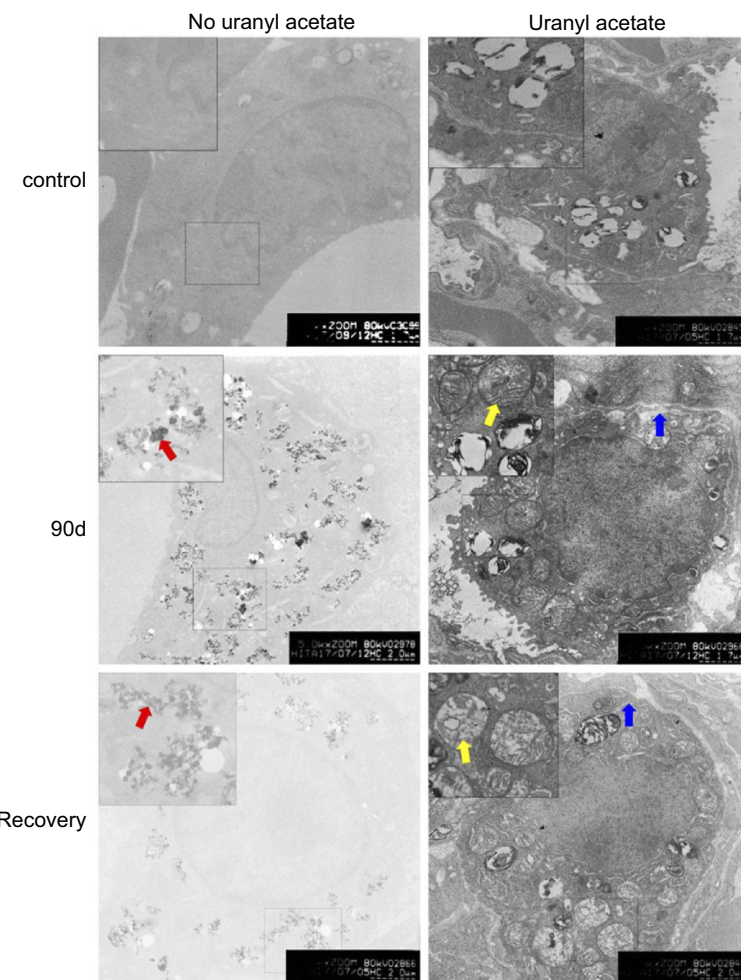


Figure 5 Representative TEM images of lung cells in rats after Carbon black (CB) inhalation and recovery (6000 \times). Inset: a higher magnification of the lung tissue (12,000 \times). Alveolar type II epithelial cells in control (Right, staining by uranyl acetate and lead citrate); macrophages in the lung of rats (Left, no uranyl acetate and lead citrate staining). The arrows indicate: Red arrow, CB particles in a lung macrophage; Yellow arrow, mitochondria; Blue arrow, rough endoplasmic reticulum.

Table 2 The cytokines levels in the lung supernatant of rats (pg/mg protein)

Cytokines	Control	Carbon black (CB)	Recovery
IL-6	11.57 \pm 4.23	19.49 \pm 0.89*	12.58 \pm 2.55
IL-8	5.68 \pm 1.21	8.71 \pm 0.65*	8.53 \pm 1.38*
IL-17	3.75 \pm 0.55	5.54 \pm 0.48*	4.13 \pm 1.07
TNF- α	14.15 \pm 2.57	22.01 \pm 5.96*	20.93 \pm 2.31*

Notes: The number of rats in each group was six and data were shown as the mean \pm SD. * P <0.05 compared with the control group.

(WBC), Monocytes and Neutrophils, respectively, showed 1.72-, 3.13- and 2.73-fold increases, compared with the control ($t=3.547$, $P=0.001$; $t=5.825$, $P=0.000$, $t=4.325$, $P=0.000$, respectively). Though lymphocytes counts had no significant difference, the percentage of lymphocytes in peripheral blood was significantly decreased compared

with the control. For the lymphocyte subsets, the percentage of cluster of differentiation four (CD4+) Lymphocytes, and the rates of CD4+/CD8+ in CB exposure group were statistically increased compared with the control ($t=4.236$, $P=0.000$; $t=3.145$, $P=0.002$, respectively, Figure 6A). In the recovery group, neutrophils counts, CD4+, and CD4+/CD8+ were significantly decreased compared with the CB exposure group ($t=5.637$, $P=0.000$; $t=7.346$, $P=0.000$, respectively). The stimulation index of the peripheral blood lymphocytes were significantly decreased after CB exposure for 90 days and the recovery ($F=34.732$, $P=0.000$, Figure 6B). In the present study, after CB inhalation, spleen had a slight proliferation and disrupted demarcation of white and red pulp accompanying deviated central arteries. Even though the lymphocytes subsets, number of B cells, CD4+, and CD8+ cells had no significant changes (Supplemental Table S2),

Table 3 The lung function indexes after CB exposure in rats

Variables	CB		P	Recovery		P
	Control	CB exposure		Control	Recovery	
FEV1	4.23±0.25	3.09±0.55	0.006	4.37±0.37	3.35±0.44	0.007
FVC	8.36±0.37	6.77±0.47	0.015	8.04±0.25	6.98±0.19	0.001
FEV1/FVC(%)	50.59±2.55	45.64±2.74	0.003	54.35±2.37	47.99±3.39	0.008
PEF	54.25±1.35	44.74±1.73	0.018	52.33±1.45	46.74±1.69	0.013
MMF	50.07±1.09	40.25±1.77	0.004	49.37±1.97	42.88±2.09	0.022

Notes: The number of rats in each group was eight and data were shown as the mean ± SD. Multi-group comparisons of the means were carried out by a one-way analysis of variance test followed by SNK's multiple comparison tests. *P<0.05 compared with the control.

Table 4 The changes of peripheral blood cell counts and lymphocyte subsets in rats after Carbon black (CB) inhalation for 90 days

	Control	CB	Control	Recovery
WBC ($10^9/L$)	5.99±0.96	10.29±3.35*↑	6.03±1.03	7.84±2.00
Lymphocytes%	76.56±6.81	60.96±11.82*↓	75.48±7.45	72.66±4.90#↑
Monocytes%	11.97±2.92	22.99±3.27*↑	11.58±2.86	12.91±3.59#↓
Neutrophils%	12.29±2.93	18.34±7.26*↑	13.68±3.11	14.10±4.01
Monocytes ($10^9/L$)	0.72±0.15	2.25±0.83*↑	0.74±0.13	0.76±0.11
Eosinophils ($10^9/L$)	0.025±0.011	0.018±0.007	0.026±0.006	0.009±0.002*↓
Basophils ($10^9/L$)	0.025±0.008	0.008±0.006*↓	0.028±0.010	0.008±0.002*↓
Neutrophils ($10^9/L$)	0.81±0.13	2.21±0.43*↑	0.76±0.19	0.73±0.25#↓
Lymphocytes ($10^9/L$)	4.52±0.83	6.61±2.23	4.03±1.33	4.16±1.14
B Lymphocytes%	33.14±4.55	28.93±4.80	32.75±5.23	35.87±4.64#↑
CD4 ⁺ Lymphocytes%	38.22±5.09	46.00±4.60*↑	37.62±5.82	33.61±2.59#↓
CD8 ⁺ Lymphocytes%	21.82±3.17	19.56±3.00	20.77±3.25	21.46±3.95
CD4 ⁺ /CD8 ⁺	1.77±0.18	2.24±0.86*↑	1.81±0.24	1.64±0.37#↓
NK cells%	4.43±0.35	5.19±1.01	4.16±0.88	5.23±1.87

Notes: The number of rats in each group was eight and data were shown as the mean ± SD. *P<0.05 compared with the control group. #P<0.05 compared with the CB inhalation group.

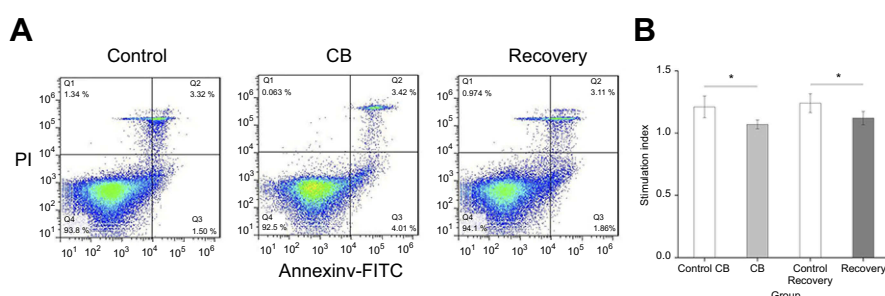


Figure 6 The stimulation index of the peripheral blood lymphocyte in the rat. Data were shown as the mean ± SD. n=8. *P<0.05 compared with the control.
Abbreviation: CB, Carbon black.

the appearance of slightly atrophic change in follicles (B cell area) and periaorticular lymphoid sheath (T cell area), abnormal lymphocytes, as well as mononuclear will result in the abnormal immune response.

No obvious changes were observed in the levels of IL-6, IL-8, IL-17, and TNF- α in serum either of the CB exposure group or the recovery group compared with the control group (data not shown).

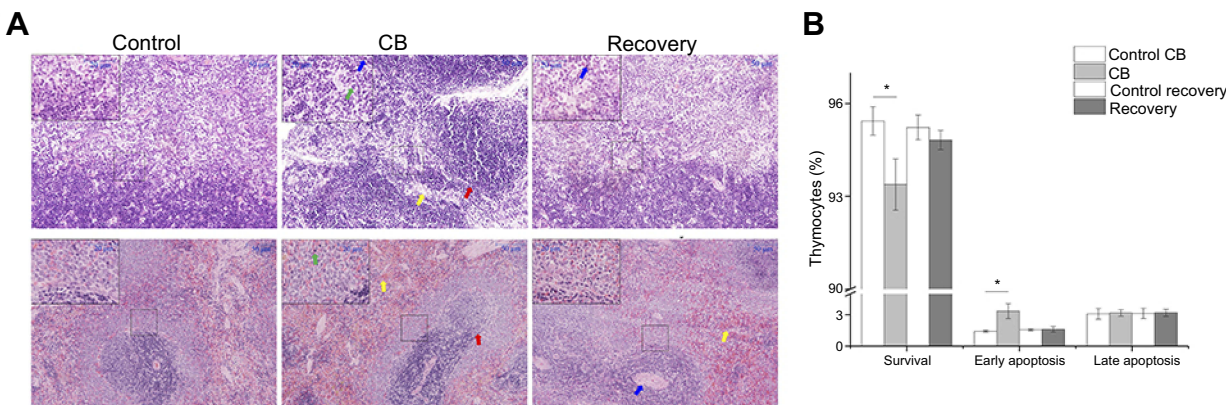


Figure 7 Representative histopathological images of the thymus and spleen tissues as well as the apoptosis of thymocyte in rats. **(A)** The above pictures representative histopathological image of the thymus in rats by HE staining ($200\times$). Inset: a higher magnification of the thymus tissue ($400\times$). The arrows indicate: Red arrow, broaden thymic cortex and narrowed thymic medulla; Yellow arrow, disrupted demarcation of medullar/cortex; Blue arrow, Monocytes, and eosinophils. The below pictures representative histopathological image of the spleen in rats by HE staining ($200\times$). Inset: a higher magnification of the thymus tissue ($400\times$). The arrows indicate: Red arrow, slight proliferated white pulp, disrupted demarcation of white and red pulp with deviated central arteries. Yellow arrow, extravasated blood Blue arrow, thickened wall of splenic arterioles. Green arrow, abnormal lymphocyte, and mononuclear cells. **(B)** The apoptosis of thymocyte detected by flow cytometry. * $P<0.05$ compared with the control group. Data were shown as the mean \pm SD. n=6.

The damages of thymus and spleen in rats after CB exposure

Compared with the control, thymus displayed slight morphologic changes in CB exposure group and recovery, including decreased cellularity in the cortex, broaden cortex and narrowed medulla, disrupted demarcation of medulla/cortex, and cytoplasmic vacuolation. Some of monocytes and eosinophils were found in CB exposure group (Figure 7A). The IL-8 levels were significantly increased in thymus of rats in CB exposure and recovery group, compared with the control. Compared with the CB exposure group, the IL-8 levels were significantly increased in recovery ($F=36.252$, $P=0.000$) (Supplemental Figure S7A and S7B).

During the observation period, early apoptotic cells had 2.36-fold increases in thymocytes after CB treatment compared with the control. The survival thymocytes were significantly decreased compared with the control ($t=3.685$, $P=0.001$). After a short-time recovery (14 days), the surviving and apoptotic thymocytes were not significantly different compared to the control ($t=3.158$, $P=0.002$, Figure 7B).

Compared with the control, spleen displayed slight morphologic changes after CB exposure and recovery which include slightly atrophic change of follicles (B-cell area) and periarteriolar lymphoid sheath (T-cell area), slightly proliferated white pulp, disrupted demarcation of white and red pulp, deviated central arteries, abnormal morphology of lymphocytes, and mononuclear, extravasated blood in white pulp and thickened wall of splenic arterioles (Figure 7A).

Discussion

Dominant PM fraction emitted into the atmosphere is carbonaceous material. CB particles are produced most often by diesel engines, burning trash, and cooking or heating stoves that burn coal, kerosene or biomass. It is fine enough to penetrate deep into the lungs, bloodstream, heart, and brain, causing inflammatory responses and other long-term health effects. A low dose (7 μg) of CB nanoparticles which avoided particle overload did not acutely aggravate an established allergic airway inflammation in mice.³⁰ However, intratracheal instillation of 162 μg CB nanoparticles resulted in increased neutrophil influx, changes in the expression of genes associated with inflammation, and genotoxicity in the lungs of C57BL/6 mice that lasted for 14 days, 28 days, and late 42 days.^{24,31,32} The important factors contributing to toxicity of inhaled particles were related to the deposition and alveolar clearance via macrophages.³³ After 30 mg/m^3 CB exposure for 90 days, the contents of CB in lung tissue were 7.09 mg by SDS-PAGE, while the calculated deposition of CB in each rat was 16 mg by MPPD.³⁴ Though there was inconsistent between calculated and detected deposition of CB in the lung of rat, SDS-PAGEbased detection could provide the relative clearance.^{29,35} After a short-time recovery, 14.10% CB accumulated was cleared from the lung, which indicated that the lungs still retain most of the particles. However, to make more detailed assessments on clearance trends over time, longer or a series of recovery periods will be required. In the present study and previous studies, the apoptosis, DNA damages, fibrosis, and inflammation

were still persistent after a short time recovery,^{36,37} which might relate with the only 14.10% CB clearance from lung and there still were deposited amounts of the CB in the lung, and then the damage to lung proceeded persistently.

The CB particles deposited in the lung could initiate the damages to the lung and other tissue. Three weeks of repeated aspiration study suggested that CB induced minimal to mild inflammation and fibrosis.³⁸ However, after exposed to 15 mg/m³ CB for 28 days, there was no induction of alveolar inflammation or fibrosis in rats.³⁹ In the present study, apoptosis, DNA damages, and a common sequence of events have emerged involving chronic inflammation, formation of granulomas, and development of fibrosis in lung interstitium and blood-gas barrier after CB exposure. The localized response of CB was mainly caused by the oxidative stress, cell death and dysfunctions in the cellular machinery.^{13,40,41}

In addition to the direct damage in the lung, the second mechanism included involvement of systemic immune response resulting in the development of tissue remodeling and fibrosis that caused lung dysfunctions. After CB exposure, we found that while the cell counts of WBC, neutrophils, and mononuclear cells were significantly increased in peripheral blood, there was no increase in eosinophils in rats. Even though there were no significant changes in lymphocytes count, the percentage of lymphocytes was significantly decreased which implied that CB might have adverse effects on the immune system. These data correlated well with the disrupted histomorphology of spleen and thymus. In peripheral blood, the increased percentages of neutrophils and monocytes were thought to be related to the inflammatory response from the affected organs. These results suggested that CB could induce systemic inflammation except for the local position of deposition. In the recovery group, the percentages of lymphocytes, CD4+, and CD4+/CD8+ were not significantly different compared with the control, whereas were significantly decreased compared with the CB exposure group. These data indicated that the systemic inflammation might partly recover but not the pulmonary damages. 14 nm or 56 nm CB nanoparticles aggravated a murine model of antigen-related airway inflammation characterized by infiltration of eosinophils, neutrophils, and mononuclear cells, and by an increase in the number of goblet cells in the bronchial epithelium.⁴² In CB exposure workers, the eosinophils were significantly higher than the control, which suggested the allergy after a long-term exposure.¹

Chemokines are secondary pro-inflammatory mediators, that is, they are typically induced by primary pro-inflammatory mediators. In the present study, the IL-6, IL-8, IL-17, and TNF- α levels were significantly increased in lung tissue but not in serum after CB exposure. The reason for suppressed cytokines release in serum might relate with the systemic immune response including the decrease in lymphocytes proliferation in peripheral blood as well as the abnormal immune organs, thymus, and spleen. In the previous study, there was no severe inflammation in the lung after exposed to CB for 28 days, however, the circulating levels of inflammatory marker proteins, IL-6, C-reactive protein, and Monocyte chemoattractant protein-1 elevated markedly in rats.³⁹ These results indicated the cytokines were more sensitive than the morphological damages induced by CB.

The systemic response of CB is more complex and affects both local and distal parts of the body by more than one mechanism. CB is likely to induce T-cell-mediated immune disorders by shifting the vulnerable balance in the system and decreasing the resistance of hosts to respiratory infections. Both the absolute number and percentage of CD4+ cells and CD8+ cells in the lymph nodes increased in CB-exposed lung-draining lymph nodes of rats.⁴³ In the present study, CD4+ cells and CD4+/CD8+ were significantly increased after CB inhalation suggesting that CB could active the T-cell-mediated immune response. However, we also found the lymphocytes proliferation decreased significantly in peripheral blood which indicated that CB exposure could induce immune suppression.

After 7 or 14 days carbon nanotubes inhalation, immune suppression, cytokine upregulation, and oxidative stress in the spleen were found even at the lower exposure levels.⁴³ The initiation of the immune response is triggered in spleen which is one of the most important lymphoid organs.⁴⁴

The thymus is a primary lymphoid organ in which bone marrow-derived T-cell precursors undergo differentiation leading to the migration of CD4+ and CD8+ selected thymocytes to the T-cell-dependent areas of peripheral lymphoid organs as the naïve T cells.^{45,46} Our data showed the percentages of the lymphocytes decreased significantly in peripheral blood whereas monocytes% and neutrophils% were significantly increased after CB exposure for 90 days which might relate with the abnormal thymus function. Another reason is that the significant decrease of lymphocyte percentage might relate with its suppress of proliferation.

Conclusion

CB could induce localized or direct, and systemic toxicity. When CB came in and contacted with the lung epithelial cells, cytokines were released. These factors attracted a large number of immune cells that damaged the lungs tissue in a systemic manner. The blood monocytes and neutrophils might also participate in this initial inflammatory response. The disrupted histomorphology of thymus and spleen resulted in the abnormal growth, differentiation, and maturation of T cells, which implemented immune suppression after chronic CB exposure. Both direct and systemic immune responses were interlinked and thus toxicity could be considered as a combined effect of both of them.

Highlights

1. CB could deposit in the lung and could not clearance within a short time.
2. CB inhalation induces granulomas and fibrosis in the lung of rats.
3. CB inhalation triggers the inflammation both in lung and immune organ.
4. Both direct and systemic immune responses are inter-linked on the toxicity of CB.

Novelty Statement

This work studied the localized or direct, and systemic immune toxicity induced by chronic carbon black inhalation in rats. We evaluated the deposition and clearance rates of CB in the lung by a rapid and sensitive method. It was clear from the present study that CB inhalation induced chronic inflammation, formation of granulomas, DNA damage, apoptosis in lung and development of fibrosis in the lung interstitium, blood-gas barrier and then lung function reduction. The above damages in the lung might partly relate to the damages of thymocytes and the immune depression.

Abbreviations

BSA, Bull Serum Albumin; CB, Carbon black; CD4+, Cluster of differentiation 4; CD8+, Cluster of differentiation 8; CRP, C-reactive protein; DE, diesel exhaust; DEPs, Diesel exhaust particles; ELISA, Enzyme-linked immunosorbent assay; FBS, Fetal bovine serum; FITC, Fluorescein isothiocyanate; IgE, Immunoglobulin E; IHC, Immunohistochemical staining; IL-1 β , Interleukin- 1 β ; IL-6, Interleukin-6; IL-8, Interleukin-8; IL-17, Interleukin-17;

MCP-1, Monocyte chemoattractant protein-1; MPPD, Multiple path particle dosimetry; NK cells, Natural killer cell; OD, Optical density; SI, Stimulation index; OTM, Olive tail moment; PE, Phycoerythrin; PHA, Phytohaemagglutinin; PM, Particulate matter; SDS-PAGE, Sodium dodecyl sulfate polyacrylamide gel electrophoresis; SPF, Specific-pathogen-free; TEM, Transmission electron microscope; TNF- α , Tumor necrosis factor alpha; Th17, T helper 17 cells; WBC, White blood cell.

Ethical standards

The animal use protocol has been reviewed and approved by the Laboratory Animal Ethical and Welfare Committee of Hebei Medical University, Shijiazhuang, China. Approval No. is IACUC-Hebmu-20160047.

Acknowledgments

This work is supported by Natural Science Foundation of China (81573190, 91643108), Natural Science Foundation of Hebei Province of China (H2015206326), and Natural Science Foundation of Education Department of Hebei Province of China (ZD2015008).

Disclosure

The authors report no conflicts of interest in this work.

References

1. Lim SS, Vos T, Flaxman AD, et al. A comparative risk assessment of burden of disease and injury attributable to 67 risk factors and risk factor clusters in 21 regions, 1990–2010: a systematic analysis for the Global Burden of Disease Study 2010. *Lancet*. 2012;380(9859):2224–2260. doi:10.1016/S0140-6736(12)61766-8
2. Orjan G, Martin K, Zdenek Z, et al. Brown clouds over South Asia: biomass or fossil fuel combustion? *Science*. 2009;323(5913):495–498. doi:10.1126/science.1164857
3. Chen J, Li C, Ristovski Z, et al. A review of biomass burning: emissions and impacts on air quality, health and climate in China. *Sci Total Environ*. 2016;579:1000–1034. doi:10.1016/j.scitotenv.2016.11.025
4. Zhang Z, Wang W, Cheng M, et al. The contribution of residential coal combustion to PM 2.5 pollution over China's Beijing-Tianjin-Hebei region in winter. *Atmos Environ*. 2017;159:147–161. doi:10.1016/j.atmosenv.2017.03.054
5. Chen S, Xu L, Zhang Y, et al. Direct observations of organic aerosols in common wintertime hazes in North China: insights into direct emissions from Chinese residential stoves. *Atmos Chem Phys*. 2017;17(2):1–32. doi:10.5194/acp-17-1259-2017
6. Liu J, Mauzerall DL, Chen Q, et al. Air pollutant emissions from Chinese households: a major and underappreciated ambient pollution source. *Proc Natl Acad Sci U S A*. 2016;113(28):7756–7761. doi:10.1073/pnas.1604537113

7. Li C, Martin RV, van Donkelaar A, et al. Trends in chemical composition of global and regional population-weighted fine particulate matter estimated for 25 years. *Environ Sci Technol.* 2017;51(19):11185–11195. doi:10.1021/acs.est.7b02530
8. Lu Z, Streets DG, Winjikul E, et al. Light absorption properties and radiative effects of primary organic aerosol emissions. *Environ Sci Technol.* 2015;49(8):4868–4877. doi:10.1021/acs.est.5b00211
9. Zhang R, Dai Y, Zhang X, et al. Reduced pulmonary function and increased pro-inflammatory cytokines in nanoscale carbon black-exposed workers. *Part Fibre Toxicol.* 2014;11:73. doi:10.1186/s12989-014-0073-1
10. Koebach A, Johansen BV, Schwarze PE, Namork E. Analytical electron microscopy of combustion particles: a comparison of vehicle exhaust and residential wood smoke. *Sci Total Environ.* 2005;346(1–3):231–243. doi:10.1016/j.scitotenv.2004.10.025
11. Nikula KJ, Snipes MB, Barr EB, Griffith WC, Henderson RF, Mauderly JL. Comparative pulmonary toxicities and carcinogenicities of chronically inhaled diesel exhaust and carbon black in F344 rats. *Fundam Appl Toxicol.* 1995;25(1):80–94.
12. IARC monographs on the evaluation of carcinogenic risks to humans. Ingested nitrate and nitrite, and cyanobacterial peptide toxins. *IARC Monogr Eval Carcinog Risks Hum.* 2010;94:v–vii, 1–412.
13. Niranjan R, Thakur AK. The toxicological mechanisms of environmental soot (black carbon) and carbon black: focus on oxidative stress and inflammatory pathways. *Front Immunol.* 2017;8:763. doi:10.3389/fimmu.2017.00763
14. Patel MM, Chillrud SN, Deepthi KC, Ross JM, Kinney PL. Traffic-related air pollutants and exhaled markers of airway inflammation and oxidative stress in New York City adolescents. *Environ Res.* 2013;121:71–78. doi:10.1016/j.envres.2012.10.012
15. Sarnat SE, Raysoni AU, Li WW, et al. Air pollution and acute respiratory response in a panel of asthmatic children along the U.S.-Mexico border. *Environ Health Perspect.* 2012;120(3):437–444. doi:10.1289/ehp.1003169
16. Ma J, Guo A, Wang S, et al. From the lung to the knee joint: toxicity evaluation of carbon black nanoparticles on macrophages and chondrocytes. *J Hazard Mater.* 2018;353:329–339. doi:10.1016/j.jhazmat.2018.04.025
17. Di Gioacchino M, Petrarca C, Lazzarin F, et al. Immunotoxicity of nanoparticles. *Int J Immunopathol Pharmacol.* 2011;24(1 Suppl):65S–71S.
18. Hussain S, Vanoirbeek JA, Hoet PH. Interactions of nanomaterials with the immune system. *Wiley Interdiscip Rev Nanomed Nanobiotechnol.* 2012;4(2):169–183. doi:10.1002/wnan.166
19. Tin Tin Win S, Yamamoto S, Ahmed S, Kakeyama M, Kobayashi T, Fujimaki H. Brain cytokine and chemokine mRNA expression in mice induced by intranasal instillation with ultrafine carbon black. *Toxicol Lett.* 2006;163(2):153–160. doi:10.1016/j.toxlet.2005.10.006
20. Frampton MW, Utell MJ, Zareba W, et al. Effects of exposure to ultrafine carbon particles in healthy subjects and subjects with asthma. *Res Rep Health Eff Inst.* 2004;126:1–47; discussion 49–63.
21. Shwe TT, Yamamoto S, Kakeyama M, Kobayashi T, Fujimaki H. Effect of intratracheal instillation of ultrafine carbon black on proinflammatory cytokine and chemokine release and mRNA expression in lung and lymph nodes of mice. *Toxicol Appl Pharmacol.* 2005;209(1):51–61.
22. de Haar C, Hassing I, Bol M, Bleumink R, Pieters R. Ultrafine carbon black particles cause early airway inflammation and have adjuvant activity in a mouse allergic airway disease model. *Toxicol Sci.* 2005;87(2):409–418. doi:10.1093/toxsci/kf255
23. Saputra D, Yoon JH, Park H, et al. Inhalation of carbon black nanoparticles aggravates pulmonary inflammation in mice. *Toxicol Res.* 2014;30(2):83–90. doi:10.5487/TR.2014.30.2.083
24. Bourdon JA, Saber AT, Jacobsen NR, et al. Carbon black nanoparticle instillation induces sustained inflammation and genotoxicity in mouse lung and liver. *Part Fibre Toxicol.* 2012;9:5. doi:10.1186/1743-8977-9-5
25. Lefebvre DE, Pearce B, Fine JH, et al. In vitro enhancement of mouse T helper 2 cell sensitization to ovalbumin allergen by carbon black nanoparticles. *Toxicol Sci.* 2014;138(2):322–332. doi:10.1093/toxsci/kfu010
26. Alessandrini F, Schulz H, Takenaka S, et al. Effects of ultrafine carbon particle inhalation on allergic inflammation of the lung. *J Allergy Clin Immunol.* 2006;117(4):824–830. doi:10.1016/j.jaci.2005.11.046
27. Dai Y, Niu Y, Duan H, et al. Effects of occupational exposure to carbon black on peripheral white blood cell counts and lymphocyte subsets. *Environ Mol Mutagen.* 2016;57(8):615–622. doi:10.1002/em.22036
28. Anjilvel S, Asgharian B. A multiple-path model of particle deposition in the rat lung. *Fundam Appl Toxicol.* 1995;28(1):41–50.
29. Wang R, Meredith AN, Lee M Jr, et al. Toxicity assessment and bioaccumulation in zebrafish embryos exposed to carbon nanotubes suspended in Pluronic(R) F-108. *Nanotoxicology.* 2016;10(6):689–698. doi:10.3109/17435390.2015.1107147
30. Lindner K, Webering S, Stroebel M, et al. Low dose carbon black nanoparticle exposure does not aggravate allergic airway inflammation in mice irrespective of the presence of surface polycyclic aromatic hydrocarbons. *Nanomaterials (Basel).* 2018;8:4.
31. Husain M, Kyjovska ZO, Bourdon-Lacombe J, et al. Carbon black nanoparticles induce biphasic gene expression changes associated with inflammatory responses in the lungs of C57BL/6 mice following a single intratracheal instillation. *Toxicol Appl Pharmacol.* 2015;289(3):573–588. doi:10.1016/j.taap.2015.11.003
32. Bourdon JA, Halappanavar S, Saber AT, et al. Hepatic and pulmonary toxicogenomic profiles in mice intratracheally instilled with carbon black nanoparticles reveal pulmonary inflammation, acute phase response, and alterations in lipid homeostasis. *Toxicol sci.* 2012;127(2):474–484. doi:10.1093/toxsci/kfs119
33. Pauluhn J. Poorly soluble particulates: searching for a unifying denominator of nanoparticles and fine particles for DNEL estimation. *Toxicology.* 2011;279(1–3):176–188. doi:10.1016/j.tox.2010.10.009
34. Schwotzer D, Ernst H, Schaudien D, et al. Effects from a 90-day inhalation toxicity study with cerium oxide and barium sulfate nanoparticles in rats. *Part Fibre Toxicol.* 2017;14(1):23. doi:10.1186/s12989-017-0204-6
35. Wang R, Mikoryak C, Chen E, Li S, Pantano P, Draper RK. Gel electrophoresis method to measure the concentration of single-walled carbon nanotubes extracted from biological tissue. *Anal Chem.* 2009;81(8):2944–2952. doi:10.1021/ac802485n
36. Jacobsen NR, Moller P, Jensen KA, et al. Lung inflammation and genotoxicity following pulmonary exposure to nanoparticles in ApoE^{-/-} mice. *Part Fibre Toxicol.* 2009;6:2. doi:10.1186/1743-8977-6-2
37. Kyjovska ZO, Jacobsen NR, Saber AT, et al. DNA damage following pulmonary exposure by instillation to low doses of carbon black (Printex 90) nanoparticles in mice. *Environ Mol Mutagen.* 2015;56(1):41–49. doi:10.1002/em.21888
38. Teeguarden JG, Webb-Robertson BJ, Waters KM, et al. Comparative proteomics and pulmonary toxicity of instilled single-walled carbon nanotubes, crocidolite asbestos, and ultrafine carbon black in mice. *Toxicol Sci.* 2011;120(1):123–135. doi:10.1093/toxsci/kfq363
39. Niwa Y, Hiura Y, Sawamura H, Iwai N. Inhalation exposure to carbon black induces inflammatory response in rats. *Circ J.* 2008;72(1):144–149.
40. Levy LS, Chaudhuri I, Morfeld P, McCunney R. Comments on induction of inflammasome-dependent pyroptosis by carbon black nanoparticles. *J Biol Chem.* 2011;286(38):le17; author reply le18. doi:10.1074/jbc.L111.238519

41. Reisetter AC, Stebounova LV, Baltrusaitis J, et al. Induction of inflammasome-dependent pyroptosis by carbon black nanoparticles. *J Biol Chem.* 2011;286(24):21844–21852. doi:10.1074/jbc.M111.238519
42. Inoue K, Takano H, Yanagisawa R, et al. Effects of nano particles on antigen-related airway inflammation in mice. *Respir Res.* 2005;6:106. doi:10.1186/1465-9921-6-106
43. Yang HM, Antonini JM, Barger MW, et al. Diesel exhaust particles suppress macrophage function and slow the pulmonary clearance of Listeria monocytogenes in rats. *Environ Health Perspect.* 2001;109(5):515–521. doi:10.1289/ehp.01109515
44. Mitchell LA, Gao J, Wal RV, Gigliotti A, Burchiel SW, McDonald JD. Pulmonary and systemic immune response to inhaled multiwalled carbon nanotubes. *Toxicol Sci.* 2007;100(1):203–214. doi:10.1093/toxsci/kfm196
45. Mebius RE, Kraal G. Structure and function of the spleen. *Nat Rev Immunol.* 2005;5(8):606–616. doi:10.1038/nri1669
46. Savino W. The thymus is a common target organ in infectious diseases. *PLoS Pathog.* 2006;2(6):e62. doi:10.1371/journal.ppat.0020062

Supplementary materials

Table S1 The organ coefficients after CB exposure in rat (g/g body weight).

Tissues	CB			P	Recovery		P
	Control	CB exposure			Control	Recovery	
Liver	0.0320±0.0015	0.0322±0.0012		0.859	0.0345±0.0078	0.0323±0.0032	0.894
Kidney	0.0064±0.0003	0.0063±0.0003		0.457	0.0059±0.0005	0.0060±0.0008	0.792
Heart	0.0032±0.0002	0.0033±0.0002		0.782	0.0033±0.0003	0.0036±0.0003	0.076
Brain	0.0032±0.0003	0.0036±0.0003*		0.018	0.0033±0.0004	0.0037±0.0005	0.069
Lung	0.0034±0.0004	0.0042±0.0005*		0.004	0.0034±0.0003	0.0042±0.0008*	0.038
Spleen	0.0016±0.0002	0.0018±0.0003		0.226	0.0018±0.0007	0.0017±0.0003	0.743
Testis	0.0072±0.0013	0.0058±0.0037		0.361	0.0068±0.0015	0.0067±0.0021	0.922

Notes: The number of rats in each group was 8 and data were shown as the means ± SD (standard deviation). Multi-group comparisons of the means were carried out by a one-way analysis of variance test followed by SNK's multiple comparison tests. * $P<0.05$ compared with the control.

Table S2 The lymphocyte phenotype of spleen (%).

Groups	B	CD4+	CD8+	CD4+/CD8+	NK
Control	41.42±3.42	29.40±2.09	18.44±1.58	1.60±0.21	3.83±0.75
CB	43.35±2.79	29.06±1.35	18.22±1.30	1.61±0.16	3.23±0.61
Recovery	41.18±3.77	29.66±2.39	18.03±1.72	1.64±0.04	3.99±0.83

Notes: The number of rats in each group was 8 and data were shown as the means ± SD (standard deviation). Multi-group comparisons of the means were carried out by a one-way analysis of variance test followed by SNK's multiple comparison tests.

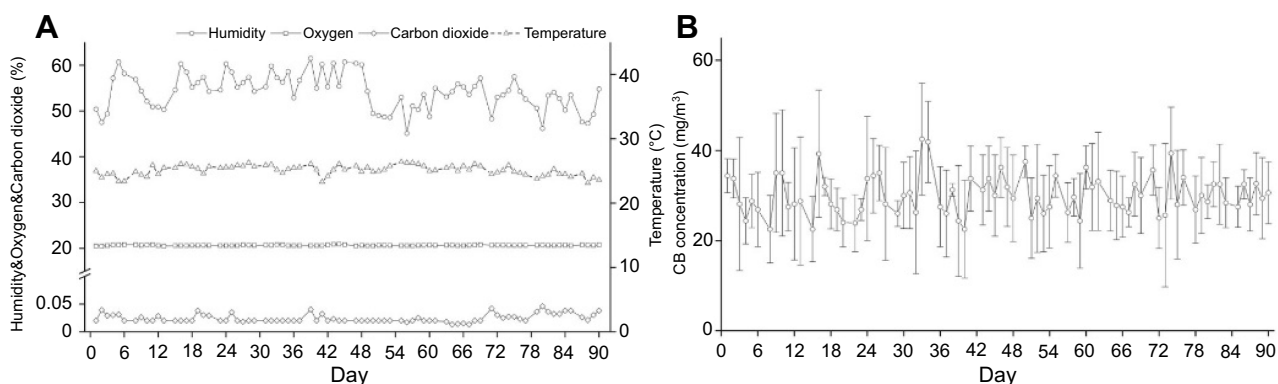


Figure S1 Environmental monitoring of the exposure chamber.

Notes: **A:** The temperature, humidity, concentration of CO₂ and O₂ in the exposure chamber during the inhalation; **B:** The concentration of CB aerosol in the exposed chamber during the inhalation.

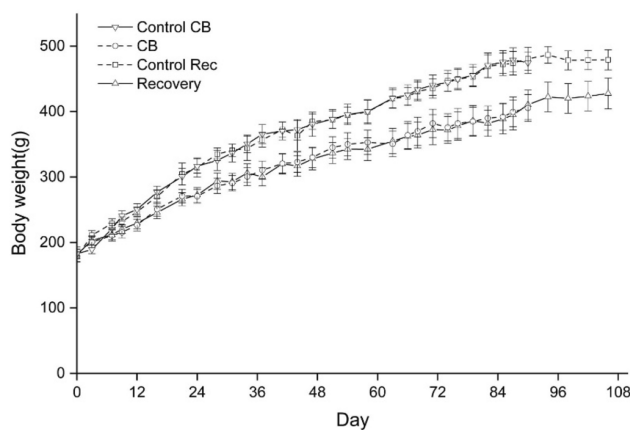


Figure S2 Changes of the body weight of rats during the inhalation and recovery.

Notes: From Day 21, statistically significant differences of body weight were found between CB exposure group and the control group. In the recovery group, the body weight of rats still significant lower than the control. Data were shown as the mean \pm SD (standard deviation). n=8.

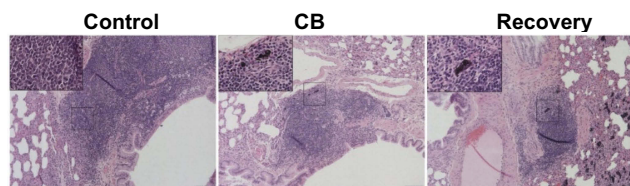


Figure S3 Representative histopathology of the pulmonary lymph node in rats by HE staining (100 \times).

Notes: A higher magnification of the lung tissue (400 \times).

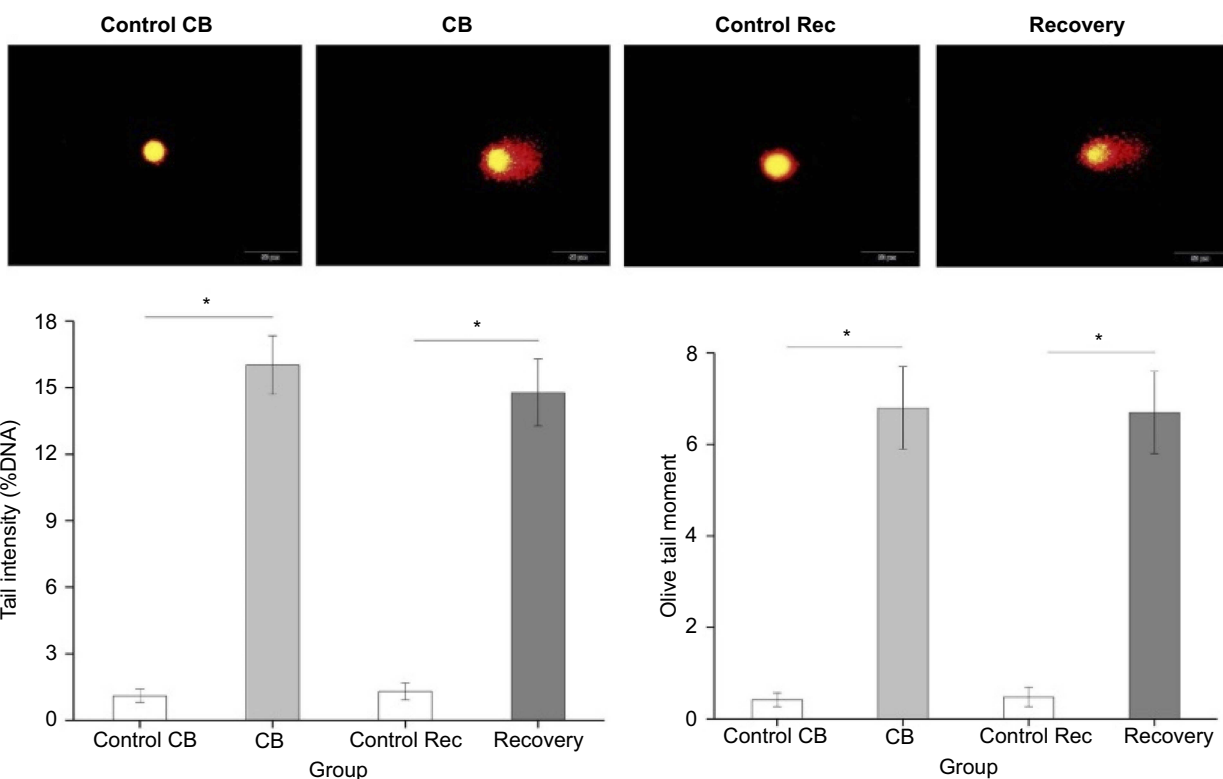


Figure S4 The DNA damages in lung tissue of rats by Comet assay.

Notes: The number of rats in each group was 6 and data were shown as the mean \pm SD (standard deviation). Multi-group comparisons of the means were carried out by a one-way analysis of variance test followed by SNK's multiple comparison tests. *P<0.05 compared with the control group. #P<0.05 compared with the CB exposure group.

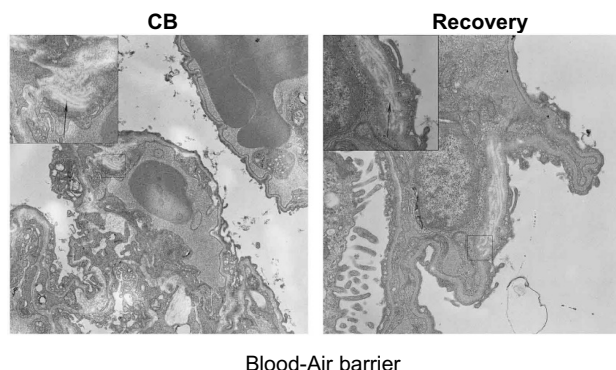


Figure S5 Representative TEM images of blood-gas barrier in rats (6000 \times).

Notes: A higher magnification of the lung tissue (12000 \times). The arrows indicate fibrosis of blood-gas barrier.

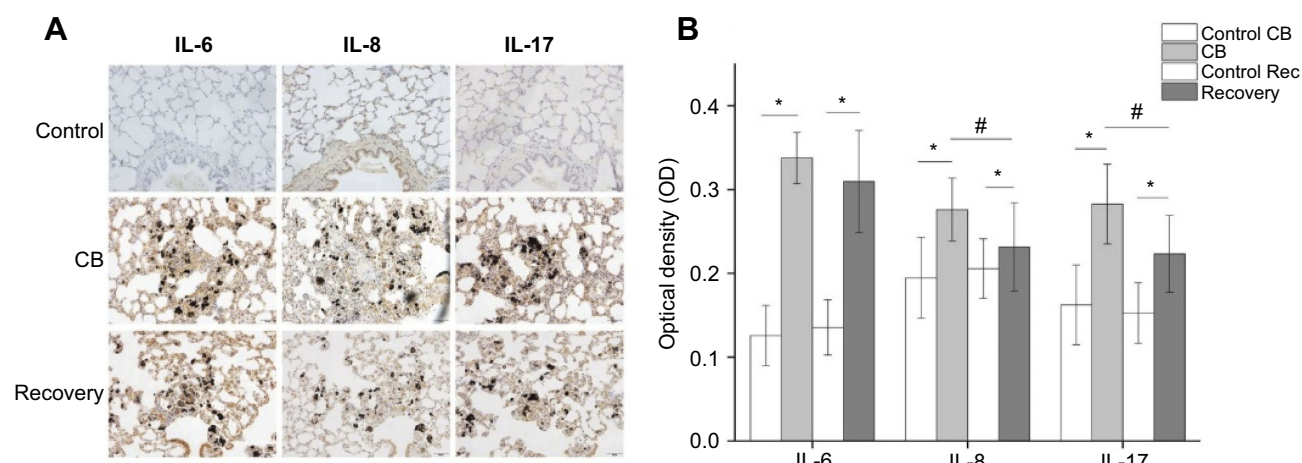


Figure S6 The cytokine levels of lung tissue by IHC.

Notes: **A:** The representative graphs of the cytokines expression in lung tissue (200 \times). The cytokines positive cells displayed brownish yellow granules. In lung cells, they were located mainly in the cytoplasm and karyon. **B:** The statistic analysis of the cytokine levels. The number of rats in each group was 6 and data were shown as the mean \pm SD (standard deviation). Multi-group comparisons of the means were carried out by a one-way analysis of variance test followed by SNK's multiple comparison tests.

*P<0.05 compared with the control group. #P<0.05 compared with the CB exposure group.

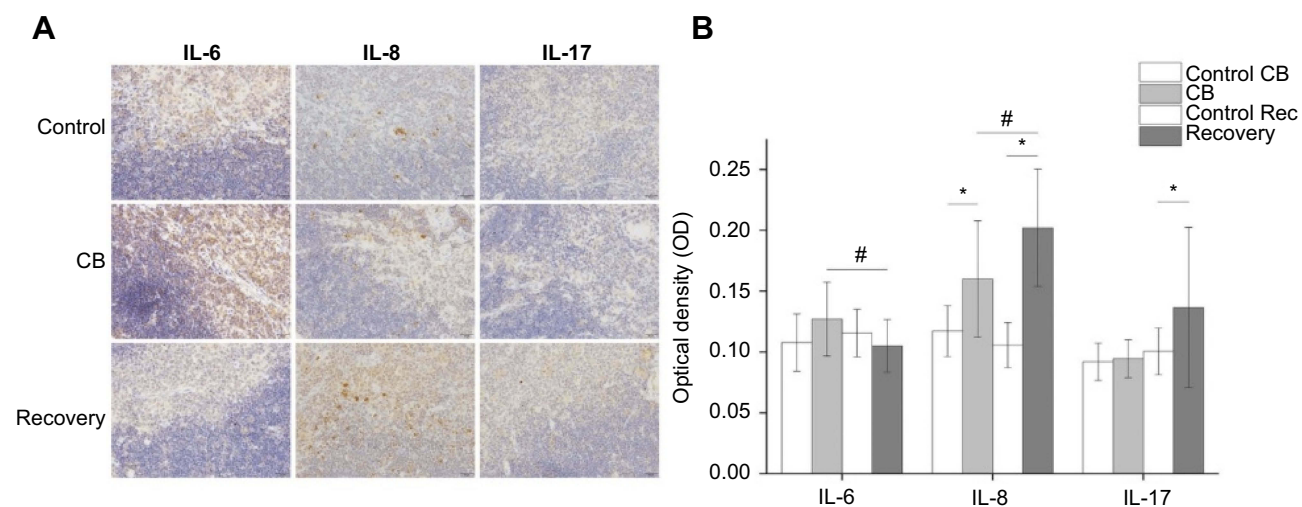


Figure S7 The cytokine levels of thymus tissue by IHC.

Notes: **A:** The representative graphs of the cytokines expression in thymus tissue (400 \times). The cytokines positive cells displayed brownish yellow granules. In thymus cells, they were located mainly in the cytoplasm and karyon. **B:** The statistic analysis of the cytokine levels. The number of rats in each group was 6 and data were shown as the mean \pm SD (standard deviation). Multi-group comparisons of the means were carried out by a one-way analysis of variance test followed by SNK's multiple comparison tests.

*P<0.05 compared with the control group. #P<0.05 compared with the CB exposure group.

International Journal of Nanomedicine**Dovepress****Publish your work in this journal**

The International Journal of Nanomedicine is an international, peer-reviewed journal focusing on the application of nanotechnology in diagnostics, therapeutics, and drug delivery systems throughout the biomedical field. This journal is indexed on PubMed Central, MedLine, CAS, SciSearch®, Current Contents®/Clinical Medicine,

Journal Citation Reports/Science Edition, EMBase, Scopus and the Elsevier Bibliographic databases. The manuscript management system is completely online and includes a very quick and fair peer-review system, which is all easy to use. Visit <http://www.dovepress.com/testimonials.php> to read real quotes from published authors.

Submit your manuscript here: <https://www.dovepress.com/international-journal-of-nanomedicine-journal>